Experimental study of the absorption of acid gases in porous particles impregnated with aqueous alkanolamide solutions

Hogendoorn, J.A.; Swaaij, W.P.M. van; Versteeg, G.F.

Published in:
Chemical Engineering Science

DOI:
10.1016/0009-2509(94)00146-4

Publication date:
1994

Pergamon

Chemical Engineering Science, Vol. 49, No. 20, pp. 3421–3438, 1994

0009–2509/94 $7.00 + 0.00

0009–2509(94)00146–4

EXPERIMENTAL STUDY OF THE ABSORPTION OF ACID GASES IN POROUS PARTICLES IMPREGNATED WITH AQUEOUS ALKANOLAMINE SOLUTIONS

J. A. HOGENDOORN, W. P. M. VAN SWAAIJ and G. F. VERSTEEG
Department of Chemical Engineering, Twente University of Technology, P.O. Box 217, 7500 AE Enschede, Netherlands

(*Received* 16 *January* 1994; *accepted for publication* 19 *April* 1994)

Abstract—In the present study the absorption behaviour and the equilibria of CO_2 and H_2S in porous α- and γ-alumina particles impregnated with inert solutions and alkanolamine solutions were investigated. From the equilibrium data it could be concluded that for CO_2 and H_2S also adsorption on the internal surface of liquid filled γ-alumina particles occurs. The experimental absorption rate data were compared with theoretical data obtained with an absorption model, which describes the mass transport accompanied by chemical reaction in porous particles impregnated with reactive solutions. The CO_2 and H_2S alkanolamine data necessary for this model were taken from literature, while the tortuosity and porosity were experimentally determined. The model could describe the experimentally observed absorption rates satisfactorily. Discrepancies mainly occurred for the process conditions where equilibrium was approached. These deviations probably must be attributed to the calculation of the equilibrium compositions (no correction for non-idealities) and the accuracy of the available thermodynamic data.

1. INTRODUCTION

Various gas–liquid processes are successfully applied in industry to separate components from gas mixtures. The absorption of the gaseous compounds in the liquid can be purely physical, but often chemically reactive species are added to the liquid. Chemically reactive components in the liquid increase the gas absorption capacity while simultaneously an enhancement of the gas absorption rate may occur. Both phenomena contribute to a better performance of the separation process. A well-known class of chemically reactive liquids applied in these processes are aqueous alkanolamine solutions which are used for the removal of CO_2 and/or H_2S from industrial gases.

Besides the solvent, the gas–liquid contactor also influences the efficiency of a separation process. Usually, a tray column or a packed column is used to realize the gas–liquid contact, however, on laboratory scale special reactors were developed to optimize specific absorption processes. Examples of such reactors are the cyclone spray scrubber and the centrifugal reactor (Versteeg and van Swaaij, 1987); Schrauwen and Thoenes, 1988; Bosch *et al.*, 1989b). These special reactors often have specific drawbacks in comparison to traditional absorbers (Bosch *et al.*, 1989b), but in some situations they might be advantageous. Especially, for the selective removal of H_2S from natural gas which also contains CO_2, the aforementioned reactors offer promising possibilities.

A new method for the continuous separation of gases with reactive liquids was proposed by Hogendoorn *et al.* (1993). Their idea was to impregnate the reactive absorption liquid in small porous particles which can be fluidized. The porous particles are used as liquid carriers, in which diffusion and simultaneous reaction of the gaseous components take place. Hogendoorn *et al.* (1993) showed that, from a theoretical point of view, impregnated small particles can effectively be used to remove gases selectively. By circulating the impregnated particles from an absorber to a desorber unit a new type of continuous separation process can be obtained. The particles can be kept in motion by various kinds of gas–solid contactors, like e.g. a bubbling fluidized bed, a riser or a trickle flow reactor.

Before studying the absorption behaviour in these types of reactors experiments in a model reactor where the particles are fixed are preferred. The problems involved with the handling of the flowing solid phase can be avoided and the absorption characteristics in the particles can be studied in more detail.

Physical absorption in liquid impregnated particles accompanied by adsorption on the internal surface of the particles has both theoretically and experimentally been studied by several authors (Edeskuty and Amundson, 1952; Ma and Evans, 1968; Komiyama and Smith, 1974a, b; Leyva-Ramos and Geankoplis, 1985; Lee *et al.*, 1993). In the experimental studies the particles were suspended in a liquid which was stirred to reduce possible external mass transfer resistances. A pulse of a fluid tracer was added to the suspension and the tracer concentration was continuously monitored. For systems with linear adsorption isotherms effective diffusion coefficients could be derived by fitting the experimental results to analytical solutions (Crank, 1976; Komiyama and Smith, 1974a, b; Prasher and Ma, 1977). Komiyama

and Smith (1974a, b) concluded that surface adsorption and diffusion significantly increased the absorption rate if the tracer in the liquid adsorbs on the internal surface of the particles. Prasher and Ma (1977) supposed that a dynamic equilibrium existed between the adsorbed molecules and the liquid in the pore. However, according to Prasher and Ma (1977), surface diffusion was not likely to occur in liquid filled porous particles because the adsorbed molecule usually is surrounded by a large number of solvent molecules. Therefore, the so-called "hopping mechanism" necessary for the surface transport cannot occur. By assuming immobilized adsorbed molecules, a dynamic equilibrium and a linear adsorption isotherm, they found that the diffusivity of (relatively large) tracer molecules in the liquid in the pores was sterically hindered and decreased with the ratio of the average pore radius to the solute molecular radius. Unfortunately, theoretical approximations were used to estimate important parameters like the molecular diffusivity of the tracer in the liquid and the tortuosity of the porous material.

The present contribution verifies whether the model proposed by Hogendoorn *et al.* (1993) can be used to describe the experimentally observed absorption rates of CO_2 and H_2S in porous particles impregnated with reactive alkanolamine solutions. Contrary to the absorption rate experiments presented in literature the absorbed component in the present study was not a liquid but a gas. Absorption rate experiments were carried out with large α- and γ-alumina particles. The α-alumina material was chosen because in many situations it can be considered as chemically inert, while γ-alumina was chosen because of the frequent application in fluidization processes. The alkanolamines used were, with increasing reaction rate towards CO_2, respectively, MethylDiEthanolAmine (MDEA), DiEthylMonoEthanolAmine (DEMEA) and MonoEthanolAmine (MEA). The reaction rate of H_2S with all three alkanolamines can be considered instantaneous with respect to mass transport.

Physical absorption experiments of CO_2 and N_2O in particles impregnated with non-reactive liquids were carried out to obtain the tortuosity of the porous particles. N_2O is often used to estimate the diffusivity and solubility of CO_2 in reactive liquids by means of the well accepted "N_2O–CO_2" analogy (Laddha *et al.*, 1981).

Also equilibrium experiments were carried out and compared with the data from literature for the homogeneous liquid system. In this way the interaction of the gases with the liquid support could be investigated.

2. THEORY

2.1. *Model description*

If a gaseous reactant A absorbs in a liquid filled porous sphere, where it reacts with component B according to the reaction

$$A + \gamma_b B \Leftrightarrow |\gamma_c| C + |\gamma_d| D \quad \gamma_b \geqslant 0;\ \gamma_c \text{ and } \gamma_d \leqslant 0 \tag{1}$$

with the kinetics

$$R_A = k_{n,m}[A]^n[B]^m - k_{p,q}[C]^p[D]^q \tag{2}$$

the mass balance for each component can be described by (Hogendoorn *et al.*, 1993):

$$\varepsilon_p \frac{\partial [i]}{\partial t} = \frac{\varepsilon_p}{q} \frac{D_i}{r^2} \frac{\partial}{\partial r}\left(r^2 \frac{\partial [i]}{\partial r}\right) - \varepsilon_p \gamma_i R_A, \quad i = \text{A, B, C or D.} \tag{3}$$

If the gas A adsorbs on the internal surface of the particle and forms A_{ads}, this component must be incorporated in the model. If it is assumed that the adsorption rate is instantaneously fast and that A is reversibly adsorbed, the adsorption isotherm describes the relation between A and A_{ads} at any point and time inside the particle. Usually, the adsorption isotherm can be represented by a Langmuir adsorption isotherm, which is given by

$$[A]_{ads} = \frac{c_1[A]}{1 + c_1[A]} c_2. \tag{4}$$

The dimension of $[A]_{ads}$ is generally mol $m^{-2}_{surface}$, but in the present model it seemed more convenient to define $[A]_{ads}$ as the number of moles adsorbed per unit pore volume. Herewith the dimensions of all components are identical which results in a straightforward interpretation of the equilibrium experiments. Component A_{ads} is incorporated in the mass balance for A which is now described by eq. (5):

$$\frac{\partial [A]}{\partial t} + \frac{\partial [A]_{ads}}{\partial t} = \frac{D_a}{qr^2} \frac{\partial}{\partial r}\left(r^2 \frac{\partial [A]}{\partial r}\right) + \frac{D_{a,ads}}{r^2} \frac{\partial}{\partial r}\left(r^2 \frac{\partial [A]_{ads}}{\partial r}\right) - R_A. \tag{5}$$

The boundary and initial conditions for the liquid filled particle are given by relations (4) and (6)–(9).

$$[i]_{t=0} = \text{constant}, \quad 0 \leqslant r \leqslant r_1, \quad i = \text{A, B, C or D} \tag{6}$$

$$[A]_{r_1} = m[A]_g \tag{7}$$

$$\left.\frac{\partial [i]}{\partial r}\right|_{r_1} = 0, \text{ non-volatile components B, C and D} \tag{8}$$

$$\left.\frac{\partial [i]}{\partial r}\right|_{r=0} = 0, \quad i = \text{A, B, C or D.} \tag{9}$$

If the reaction rate is infinitely fast in comparison with the diffusion in the particle, the balance for component A is, for all stoichiometric coefficients equal to 1, given by

$$\frac{\partial [A]}{\partial t} + \frac{\partial [A]_{ads}}{\partial t} + \frac{\partial [C]}{\partial t} = \frac{D_a}{qr^2} \frac{\partial}{\partial r}\left(r^2 \frac{\partial [A]}{\partial r}\right) + \frac{D_{a,ads}}{r^2} \frac{\partial}{\partial r}\left(r^2 \frac{\partial [A]_{ads}}{\partial r}\right) + \frac{D_c}{qr^2} \frac{\partial}{\partial r}\left(r^2 \frac{\partial [C]}{\partial r}\right) \tag{10}$$

and for component D and B by

$$\frac{\partial[\mathrm{D}]}{\partial t}-\frac{\partial[\mathrm{C}]}{\partial t}=\frac{\mathrm{D}_d}{qr^2}\frac{\partial}{\partial r}\left(r^2\frac{\partial[\mathrm{D}]}{\partial r}\right)-\frac{\mathrm{D}_c}{qr^2}\frac{\partial}{\partial r}\left(r^2\frac{\partial[\mathrm{C}]}{\partial r}\right) \tag{11}$$

$$\frac{\partial[\mathrm{B}]}{\partial t}+\frac{\partial[\mathrm{C}]}{\partial t}=\frac{\mathrm{D}_b}{qr^2}\frac{\partial}{\partial r}\left(r^2\frac{\partial[\mathrm{B}]}{\partial r}\right)+\frac{\mathrm{D}_c}{qr^2}\frac{\partial}{\partial r}\left(r^2\frac{\partial[\mathrm{C}]}{\partial r}\right). \tag{12}$$

Because equilibrium is established at any time and place within the liquid in the particle the concentration of component C is calculated according to relation (13):

$$K=\frac{[\mathrm{C}]\,[\mathrm{D}]}{[\mathrm{A}]\,[\mathrm{B}]}. \tag{13}$$

The boundary conditions for components B and D become

$$\mathrm{D}_b\frac{\partial[\mathrm{B}]}{\partial r}\bigg|_{r_1}+\mathrm{D}_c\frac{\partial[\mathrm{C}]}{\partial r}\bigg|_{r_1}=0 \tag{14}$$

and

$$\mathrm{D}_d\frac{\partial[\mathrm{D}]}{\partial r}\bigg|_{r_1}-\mathrm{D}_c\frac{\partial[\mathrm{C}]}{\partial r}\bigg|_{r_1}=0. \tag{15}$$

During the experiments the particles are present in a closed reactor which is initially evacuated. Next the vapour pressure of the liquid in the particles is allowed to establish. At $t = 0$ s pure gas is added instantaneously to a partial pressure P_0. If it is assumed that the ideal gas law is applicable, the pressure decrease is calculated with the following mass balance:

$$\frac{V_g}{RT}\frac{\partial P}{\partial t}=-J_a a_s V_{\mathrm{tot}} \tag{16}$$

in which the specific contact area for spheres is expressed by

$$a_s=\frac{3\varepsilon_s}{r_1} \tag{17}$$

and the flux J_a is for a finite rate reaction given by

$$J_a=\mathrm{D}_a\frac{\varepsilon_p}{q}\frac{\partial[\mathrm{A}]}{\partial r}\bigg|_{r_1}+\varepsilon_p\mathrm{D}_{a,\mathrm{ads}}\frac{\partial[\mathrm{A}]_{\mathrm{ads}}}{\partial r}\bigg|_{r_1} \tag{18}$$

while for an infinitely fast reaction the flux J_a is given by relation (19):

$$J_a=\mathrm{D}_a\frac{\varepsilon_p}{q}\frac{\partial[\mathrm{A}]}{\partial r}\bigg|_{r_1}+\varepsilon_p\mathrm{D}_{a,\mathrm{ads}}\frac{\partial[\mathrm{A}]_{\mathrm{ads}}}{\partial r}\bigg|_{r_1}+\mathrm{D}_c\frac{\varepsilon_p}{q}\frac{\partial[\mathrm{C}]}{\partial r}. \tag{19}$$

The initial condition of eq. (16) is given by

$$P_{t=0}=P_0. \tag{16a}$$

Equation (16) can be solved simultaneously with the micro balances for the components in the particle to obtain the theoretical time–pressure curve (see Hogendoorn *et al.*, 1993).

2.2. *Particle geometry*

In the model description of Section 2.1 it is assumed that the particles are spherical. However, the particles used in the experimental study of the gas absorption rate were cylindrical with a length to diameter ratio of about 1.

Ma and Evans (1968) presented theoretically calculated dimensionless time–accumulation curves for physical absorption in particles of various shapes. From their work it can be concluded that particles with the same volume to surface ratio show, especially at low dimensionless accumulations, practically the same absorption rate. The curves for cylinders, with a length to diameter ratio of 1, and spheres nearly coincide over the entire absorption period. The same phenomenon is known for catalytic first-order irreversible reactions. The analytical degree of utilization for particles with the same volume to surface ratio is, especially at high Thiele moduli, nearly identical (Aris, 1957).

Therefore, in the present study the cylindrical particles were approximated by a sphere with the same volume to surface ratio. For cylinders with a length to diameter ratio of 1 this means that the cylinder can be approximated by a sphere with an identical radius. Possible discrepancies between the theoretical time-pressure curves for the cylindrical and spherical geometry are expected to be small and will probably occur only at intermediate to high dimensionless accumulations.

2.3. *Reaction scheme*

If CO_2 absorbs in an aqueous tertiary alkanolamine solution multiple reactions occur. The reactions of importance for CO_2 with aqueous MDEA are:

$$\mathrm{CO_2+H_2O+MDEA \Leftrightarrow MDEAH^+ + HCO_3^-}, \tag{20}$$

$$K_{\mathrm{CO_2}}=\frac{[\mathrm{MDEAH^+}]\,[\mathrm{HCO_3^-}]}{[\mathrm{MDEA}]\,[\mathrm{CO_2}]}$$

$$\mathrm{CO_2+OH^- \Leftrightarrow HCO_3^-}, \quad K_1=\frac{[\mathrm{HCO_3^-}]}{[\mathrm{OH^-}]\,[\mathrm{CO_2}]} \tag{21}$$

$$\mathrm{HCO_3^- + OH^- \Leftrightarrow CO_3^{2-} + H_2O}, \tag{22}$$

$$K_2=\frac{[\mathrm{CO_3^{2-}}]\,[\mathrm{H_2O}]}{[\mathrm{HCO_3^-}]\,[\mathrm{OH^-}]}$$

$$\mathrm{MDEAH^+ + H_2O \Leftrightarrow MDEA + H_3O^+}, \tag{23}$$

$$K_a=\frac{[\mathrm{MDEA}]\,[\mathrm{H_3O^+}]}{[\mathrm{MDEAH^+}]\,[\mathrm{H_2O}]}$$

$$\mathrm{2H_2O \Leftrightarrow H_3O^+ + OH^-}, \tag{24}$$

$$K_w=\frac{[\mathrm{H_3O^+}]\,[\mathrm{OH^-}]}{[\mathrm{H_2O}]^2}.$$

The reactions of CO_2 occurring in an aqueous tertiary alkanolamine DEMEA solution are similar to that of MDEA. The first two reactions are reactions of

finite rate, while the following three only involve a proton transfer and are considered instantaneous with respect to mass transfer. In a model based on the Higbie penetration theory, Glasscock and Rochelle (1989) and Littel *et al.* (1991a) showed that the influence of reactions (21)–(24) was for tertiary amines negligible for the conditions the authors applied.

Primary or secondary amines react directly with CO_2 and for e.g. an aqueous MEA solution the main reaction is now given by

$$CO_2 + 2MEA \Leftrightarrow MEACOO^- + MEAH^+, \quad K_{CO_2} = \frac{[MEACOO^-][MEAH^+]}{[MEA]^2[CO_2]}. \tag{25}$$

The contribution of reaction (21) to the reaction rate can be neglected for primary and secondary amines compared to reaction (25). The overall equilibrium value K_{CO_2} is calculated according to

$$K_{CO_2} = \frac{K_1 K_w}{K_c K_a} \tag{26}$$

in which K_1, K_w and K_a are defined in accordance with the equations given in the reaction scheme for the tertiary amines, and K_c is the equilibrium constant for the reaction

$$MEACOO^- + H_2O \Leftrightarrow MEA + HCO_3^-, \quad K_c = \frac{[MEA][HCO_3^-]}{[MEACOO^-][H_2O]}. \tag{27}$$

The values for the equilibrium constants were obtained from literature and are summarized in Table 1. For all three alkanolamines the forward reaction is first order with respect to both CO_2 and the alkanolamines. The rate expression for the reverse reaction and the corresponding reaction rate constant were derived from the equilibrium expression and the assumption that at equilibrium $R_A = 0$ (Bosch, 1989a).

If H_2S absorbs in an aqueous alkanolamine solution (primary, secondary or tertiary) the most important reaction is

$$H_2S + Amine \Leftrightarrow HS^- + AmineH^+, \quad K_{H_2S} = \frac{[AmineH^+][HS^-]}{[Amine][H_2S]}. \tag{28}$$

For all alkanolamines this reaction can be considered instantaneous with respect to mass transfer. The overall equilibrium value, K_{H_2S}, is again comprised of various basis equilibria and calculated according to

$$K_{H_2S} = \frac{K_3}{K_a}. \tag{29}$$

In which K_3 represents the equilibrium value of the reaction

$$H_2S + H_2O \Leftrightarrow HS^- + H_3O^+, \quad K_3 = \frac{[HS^-][H_3O^+]}{[H_2S][H_2O]}. \tag{30}$$

In the model calculations the following three additional assumptions were made:

—All components in the liquid show ideal behaviour, which means that no activity coefficients were introduced in the equilibrium equations.

—The temperature in the reactor was constant. Although the reaction of CO_2 with alkanolamines is exothermic, the number of moles which was absorbed in the experiments was very small, so the temperature rise in the particles could be neglected.

—The diffusivities of the ionic species were taken equal to assure electroneutrality in the liquid phase (Littel, 1991a).

Table 1. Equilibrium constants at 298 K

Constants	Values	Reference
K_1	4.47×10^4	(Blauwhoff, 1980)
K_2	2.57×10^5	(Blauwhoff, 1980)
K_w	3.30×10^{-18}	(Blauwhoff, 1980)
$K_{a,MDEA}$	5.32×10^{-11}	(Littel, 1990a)
$K_{a,DEMEA}$	4.28×10^{-12}	(Littel, 1990a)
$K_{a,MEA}$	5.61×10^{-12}	(Blauwhoff, 1980)
$K_{c,MEA}$	6.67×10^{-4}	(Blauwhoff, 1980)
K_3	2.04×10^{-9}	(Blauwhoff, 1980)

3. EXPERIMENTAL

3.1. *Materials*

Some preliminary calculations and experiments showed that the absorption period for particles with a diameter of less than 1 mm was too short to obtain accurate experimental data. Therefore, the absorption rate experiments were carried out with large particles, whose properties are listed in Table 2. Because the length of the cylindrical particles varied slightly, the value given in Table 2 is the average of the length of 10 randomly chosen pellets. To study the effect of the basicity of the porous carriers, γ-alumina powders obtained from Aldrich were also used for the equilibrium experiments. When suspended in water these powders produce a slightly acidic, neutral or basic suspension. The pH of the aqueous suspensions of the materials is also listed in Table 2. The amines were obtained from Janssen Chimica (MEA and MDEA) and Aldrich (DEMEA) while ethanol and toluene were obtained from Merck. All chemicals were used as received.

3.2. *Impregnation of the particles*

Before impregnation, the particles or powder were dried at 200°C for one night in order to remove water. For the particles a "wet" impregnation method was used, while for the powder "dry" impregnation appeared to be necessary.

The wet impregnation consisted of the following steps. The particles were brought in a flask and the desired solution was added until the particles were completely submerged. Subsequently, the flask was evacuated to the vapour pressure. After this the particles

Table 2. Properties of the materials used

Material	Name	Manufacturer	Shape	Size	Porosity (–)	pH of aqueous suspension	BET surface area ($m^2 g^{-1}$)
γ-Al_2O_3	Al104T $\frac{1}{4}$ in	Engelhard	Cylinders	$l = 5.0$ $d = 6.46$ mm	0.58	9.8	95
γ-Al_2O_3	Al104T $\frac{1}{8}$ in	Engelhard	Cylinders	$l = 3.60$ $d = 3.22$ mm	0.58	9.8	94
α-Al_2O_3	Al3980T $\frac{1}{8}$ in	Engelhard	Cylinders	$l = 3.24$ $d = 3.21$ mm	0.53	8.4	4
γ-Al_2O_3	Weakly acidic	Aldrich	Powder	$d \sim 70\,\mu$m	0.50	4.6	161
γ-Al_2O_3	Neutral	Aldrich	Powder	$d \sim 70\,\mu$m	0.50	7.5	177
γ-Al_2O_3	Weakly basic	Aldrich	Powder	$d \sim 70\,\mu$m	0.50	9.9	156

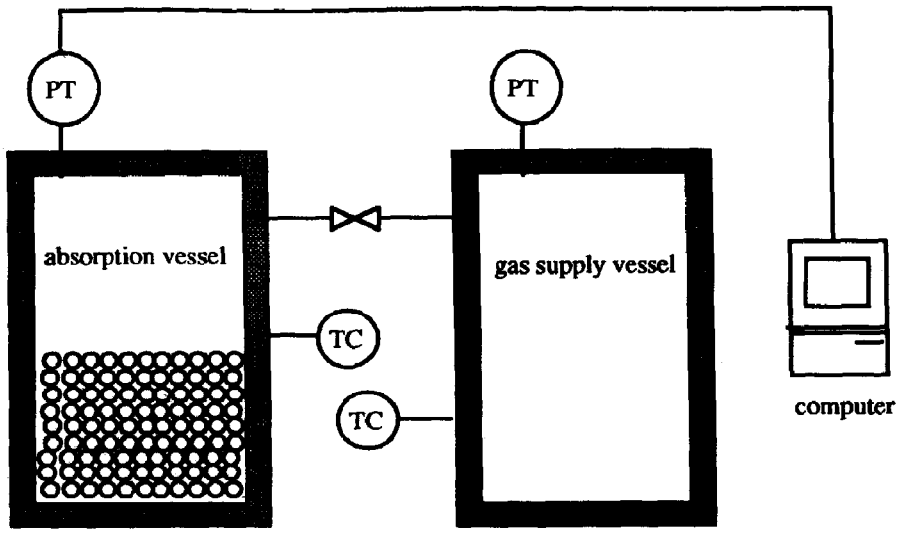

Fig. 1. Schematic representation of experimental set-up.

were stored overnight to ensure total impregnation and removal of entrapped gas. The excess of impregnation liquid was removed and the particles were ready to use.

The γ-alumina powder of Aldrich had a small pore diameter (5.8 nm) and hence very strong capillary forces can occur. These forces made it possible to impregnate the powder with the dry impregnation method. The desired solution was slowly added to the stirred powder until the powder became clotty. The impregnated powder was exposed to vacuum and stored overnight for removal of remaining entrapped gas. Thereafter the powder was impregnated a second time with the desired liquid. The amount which could be added the second time was negligible in comparison to the volume which could be impregnated the first time.

To compare the different impregnation methods for the γ-alumina, the $\frac{1}{4}$ in γ-alumina pellets (pore diameter $\pm$ 5 nm) were impregnated both wet and dry (the large particles were, in contrast to the powder, not stirred but shaken). The total amount of liquid which could be impregnated in the $\frac{1}{4}$ in γ-alumina particles was identical for both impregnation methods.

Analysis of the excess of a MDEA solution, used to impregnate γ-alumina particles with the wet impregnation method, indicated that the concentration of the amine in and outside the particles was identical to the initial concentration in the solution, which meant that no noticeable surface adsorption of the amine occurred.

3.3. *Experimental set-up and procedure*

A schematic representation of the experimental set-up is given in Fig. 1. Two double walled temperature controlled reactor cells with a calibrated volume of about 1×10^{-3} m^3 were connected via a valve. Both cells were equipped with a pressure transducer. Impregnated particles were brought in one of the cells and evacuated to the vapour pressure of the liquid in the particles. Pure gas was admitted to the other cell. At $t = 0$ the valve was opened for a short time (typically less than 3 s), and gas was allowed to flow in the

absorption vessel. The theoretical initial pressure in the absorption vessel could be calculated with the pressure drop in the gas supply vessel. In all the experiments with H_2S and also with the fast reacting CO_2–MEA system a slightly different procedure was followed. At $t = 0$ the valve was opened and kept open during the entire absorption period. To avoid a vapour stream from the absorption vessel to the gas supply vessel, a small amount of water ($\pm$ 2 ml) was added to the gas supply vessel in order to saturate the gas.

The pressure decrease in the absorption vessel was recorded with a pressure transducer, which had been connected to a computer. This method made it possible to measure the pressure with very short time intervals. To determine the equilibrium compositions, gas was, after reaching equilibrium in the absorption vessel, fed to the reactor several times up to a partial pressure of about 1 bar. All experiments were carried out with fresh unloaded porous materials at a temperature of 298 $\pm$ 1 K.

4. RESULTS AND DISCUSSION: EQUILIBRIUM EXPERIMENTS

4.1. *Particles impregnated with non-reacting liquids*

4.1.1. *Physical solubilities of* CO_2 *and* N_2O *in α-alumina pellets.* In the experiments with α-alumina the solubilities found for N_2O in the non-reacting solvents water, ethanol and toluene were within $\pm$ 10% equal to the dimensionless solubilities given in literature for the homogeneous liquid systems. The dimensionless solubility of CO_2 in with ethanol and toluene impregnated α-alumina particles agreed also satisfactorily with the literature data (see Table 3). However, the solubility of CO_2 in α-alumina impregnated with water, turned out to be substantially higher than expected. This contribution could be due to the slightly basic properties of the α-alumina. Therefore, the α-alumina was impregnated with a 0.01 M HCl solution and the measured solubility of CO_2 was nearly identical to the one found for homogeneous liquid systems.

4.1.2. *Absorption capacity of* N_2O, CO_2 *and* H_2S *in γ-alumina impregnated with non-reacting solvents.* Again the experimentally determined solubility of N_2O in γ-alumina particles impregnated with various solvents agree reasonably with the data found in literature (see Table 3). However, the absorption of CO_2 in porous γ-aluminas impregnated with non-reacting liquids was substantially higher than expected on the basis of the physical solubility. In Fig. 2 the extra "absorption" in the γ-alumina particles of Engelhard is plotted as a function of the concentration physically dissolved CO_2 in the liquid. This extra absorption in ethanol and toluene had to be caused by surface adsorption of CO_2 on γ-alumina. This is a well known phenomenon in gas–solid systems (e.g. Rosynek, 1975), but from the present experiments it can be concluded that surface adsorption of CO_2 is also of importance in γ-alumina particles impregnated with

Table 3. Dimensionless solubilities in solvents impregnated in porous particles at 298 K

Material	Supplier	Name	Gas	Solvent	Number of measurements	Experimental solubility (m)	Literature value (m)	Source
γ-alumina	Engelhard	Al104T	N_2O	Ethanol	4	2.61	3.07	IUPAC
γ-alumina	Engelhard	Al104T	N_2O	Toluene	11	3.19	3.41	Littel (1991c)
γ-alumina	Engelhard	Al104T	N_2O	2 M MDEA	3	0.46	0.51	Versteeg (1988)
α-alumina	Engelhard	Al3980T	N_2O	Ethanol	3	2.72	3.07	IUPAC
α-alumina	Engelhard	Al3980T	N_2O	Toluene	4	3.19	3.41	Littel (1991c)
α-alumina	Engelhard	Al3980T	N_2O	Water	4	0.53	0.60	Versteeg (988)
α-alumina	Engelhard	Al3980T	CO_2	Ethanol	3	3.00	2.78	Littel (1991d)
α-alumina	Engelhard	Al3980T	CO_2	Toluene	4	2.41	2.35	Littel (1991c)
α-alumina	Engelhard	Al3980T	CO_2	Water†	2	0.83	0.82	Versteeg (1988)

†0.01 M HCl solution.

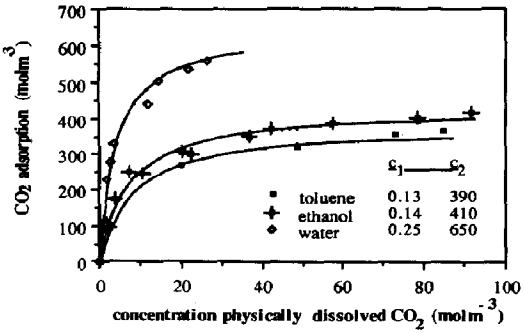

Fig. 2. CO_2 adsorption isotherm at 298 K for $\frac{1}{4}$ in γ-alumina particles impregnated with non-reactive liquids.

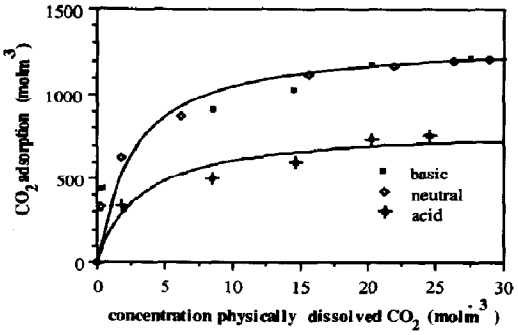

Fig. 3. CO_2 adsorption isotherm at 298 K for Aldrich powders impregnated with water.

liquids. The occurrence of such strong surface adsorption was not expected because, owing to the high solute concentration in the pores, it was assumed that practically all active adsorption places would be occupied by solute molecules. The adsorption isotherm for toluene and ethanol (see Fig. 2) was fitted with a Langmuir adsorption isotherm represented by relation (4). The extra adsorption of CO_2 in basic γ-alumina particles impregnated with water may also be partially attributed to the formation of OH^-. The OH^- can be formed as a consequence of the reaction of the γ-alumina surface with water. However, the pH of the aqueous suspensions (Table 2) indicate that the concentration of OH^- is low, so the adsorption of CO_2 probably had to be caused by adsorption on the surface.

The results of the experiments with the Aldrich powders with various surface properties support this view. The γ-alumina powders of Aldrich have similar internal surface areas and porosities and corresponding surface to porous volume ratios. The CO_2 absorption capacity for the basic and neutral aluminas of Aldrich impregnated with water are, within the experimental error, identical (see Fig. 3). If the extra absorption could be completely attributed to the OH^- formation in the liquid, the amount of absorbed CO_2 for the neutral and acidic alumina should correspond to the solubility data found for homogeneous liquid systems, while the basic material would have a higher CO_2 absorption capacity. However, not only the CO_2 absorption capacity for the basic, but also for the neutral and acidic alumina is considerably higher than the solubility data for homogeneous water systems. It is of course possible that a small amount of the extra absorption in basic aluminas is due to the reaction with OH^- in the liquid but the main contribution to the extra absorption is most likely caused by surface adsorption of CO_2.

The equilibrium isotherm of H_2S in $\frac{1}{4}$ in γ-alumina particles impregnated with water shows that this gas also adsorbs on the internal surface of this material (Fig. 4). However, in comparison with CO_2, the adsorption capacity is lower, which is probably due to the somewhat lower acidity of H_2S in relation to that of CO_2.

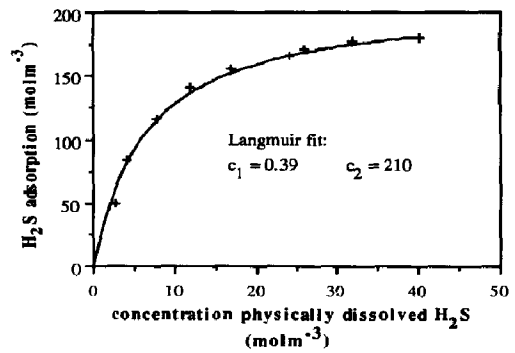

Fig. 4. H_2S adsorption isotherm at 298 K for $\frac{1}{4}$ in γ-alumina particles.

4.2. *Absorption capacity of* CO_2 *and* H_2S *in particles impregnated with reactive liquids*

Absorption equilibrium data of CO_2 in α-alumina impregnated with a 2 M MDEA solution were compared with experimental data for the homogeneous liquid system (Jou *et al.*, 1982; Bhairi, 1984). As can be seen in Fig. 5 the agreement between the present data for the impregnated solution and the data obtained by Jou *et al.* (1982) and Bhairi (1984) is satisfactory. Probably, as a consequence of the difference in purity of the alkanolamines, the discrepancy between literature data is, especially at lower CO_2 concentrations, considerable. However, these adsorption equilibrium data, in α-alumina particles impregnated with reacting, as well as non-reacting liquids, indicate that no noticeable surface adsorption of one of the components involved in the CO_2-alkanolamine reaction considered inert.

The absorption equilibrium of CO_2 in $\frac{1}{4}$ in γ-alumina pellets impregnated with a 2 M MDEA solution is given in Fig. 6. The continuous line presents the summation of the CO_2 adsorption in γ-alumina pellets impregnated with water according to the Langmuir isotherm (Fig. 2) and the (interpolated) absorption data of Jou *et al.* (1982) for a 2 M MDEA solution. The same was done for the absorption of CO_2 in Aldrich powders impregnated with a 2 M

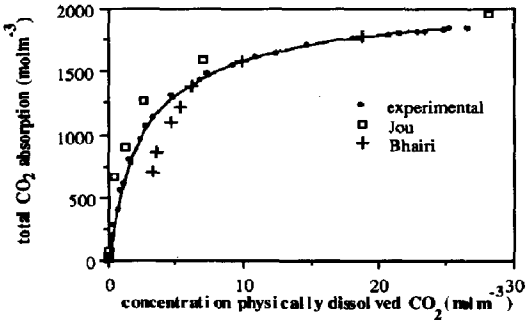

Fig. 5. CO_2 absorption isotherm for a 2 M MDEA solution impregnated in α-alumina at 298 K.

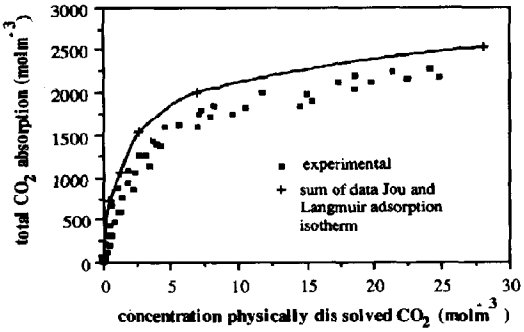

Fig. 6. CO_2 absorption isotherm at 298 K for a 2 M MDEA solution impregnated in ¼ in γ-alumina particles.

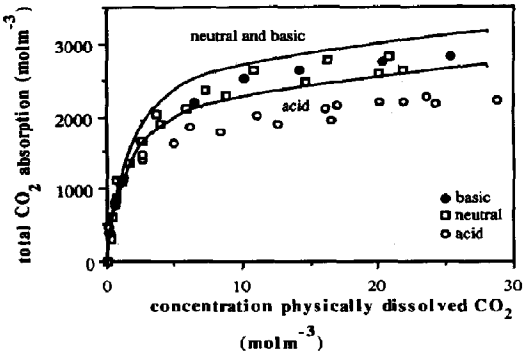

Fig. 7. CO_2 absorption isotherm at 298 K for Aldrich powders impregnated with a 2 M MDEA solution.

MDEA solution (Fig. 7). Again the continuous lines present the summation of the Langmuir adsorption isotherms (Fig. 3) and the (interpolated) data obtained by Jou *et al.* (1982) for a 2 M MDEA solution. As can be seen in Figs 6 and 7 the summation of the Langmuir adsorption isotherm and the data measured by Jou *et al.* (1982) agree reasonably well with the absorption data of CO_2 in γ-alumina particles impregnated with MDEA solutions. From these data it can be concluded that the presence of MDEA does not substantially influence the surface adsorption of CO_2.

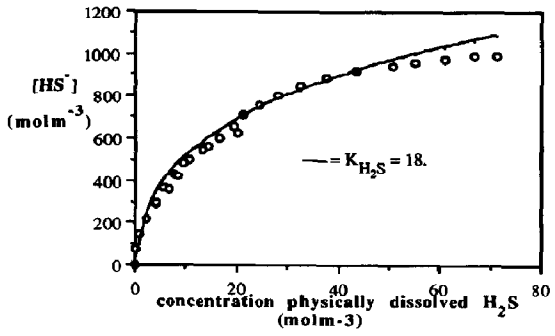

Fig. 8. H_2S absorption isotherm at 298 K for α-alumina powders impregnated with a 2 M MDEA solution.

The absorption of H_2S in α-alumina impregnated with a MDEA solution is given in Fig. 8. The absorption data can be described reasonably well, but not exactly, with an equilibrium value of $K_{H_2S} = 18$. This equilibrium value is based on ideal behaviour of all components and is not directly comparable to the value taken from literature (see Table 1, $K_{H_2S,\text{infinite dilution}} = 38.4$). If the activities of the ions are for this situation taken into account ($\gamma \leqslant 1$ for ions, $\gamma \geqslant 1$ for molecules), the concentration independent equilibrium value [see relation (31)] will even be smaller than 18.

$$K_{H_2S} = \frac{[HS^-][MDEAH^+]}{[H_2S][MDEA]} = K_{H_2S,\text{independent}} \frac{\gamma_{H_2S}\gamma_{MDEA}}{\gamma_{HS^-}\gamma_{MDEAH^+}}. \quad (31)$$

This equilibrium value ($K_{H_2S,\text{independent}} \leqslant 18$) is lower as expected on the basis of the data from literature at infinite dilution ($K_{H_2S,\text{infinite dilution}} = 38.4$), but in the available data in literature a substantial scatter can be observed which gives rise to differences in equilibrium values. This smaller equilibrium value as found in this work is therefore plausible, and was used as input parameter in the simulations of the absorption rate experiments (see Section 6.2.3).

5. EXPERIMENTAL ABSORPTION RATES IN NON-REACTING LIQUIDS

5.1. *Absorption rate experiments with non-reacting liquids*

Physical absorption rate experiments with non-reacting liquids were carried out to obtain the tortuosities of the porous supports and the surface diffusion coefficient of CO_2 in γ-alumina.

5.2. *α-alumina pellets*

The tortuosity of the α-alumina was obtained by fitting the theoretically calculated absorption rate curves to the experimental curves for CO_2 and N_2O in non-reacting liquids like water, ethanol and toluene

(see Tables 3 and 4 for data). The tortuosity of the material was determined at $q = 2.0 \pm 0.3$. With this value all physical absorption rate experiments could be simulated satisfactorily.

5.3. *γ-alumina pellets*

Physical absorption rate experiments of N_2O in toluene, ethanol and a 2 M MDEA solution were used to estimate the tortuosity of γ-alumina (see Table 4 for diffusivity data). Fitting the theoretical curves to the experimental curves resulted for the $\frac{1}{4}$ and $\frac{1}{8}$ in γ-alumina pellets in a tortuosity of $q = 2.4 \pm 0.3$.

Subsequently, the surface diffusion coefficient of CO_2 could be determined by fitting the theoretically calculated curves to experimentally obtained time-pressure data for the absorption of CO_2 in γ-alumina impregnated with non-reacting liquids. In the simulation the surface absorption of CO_2 according to the Langmuir isotherm [see eq. (4) where c_1 and c_2 as given in Fig. 2] was taken into account. The best results for all non-reacting liquids were obtained with a surface diffusion coefficient of $D_{a,ads} = 0$, indicating that the adsorbed molecules were immobile. A few examples for the various fluids and particle sizes are given in Fig. 9. The continuous line represents the numerically calculated partial pressures, while the points are the experimentally determined partial pressures. In all experiments the experimental CO_2 absorption rate was slightly lower than theoretically predicted. This could either be due to an inaccuracy in the fitted Langmuir isotherm or to the fact that the rate of the adsorption step was not instantaneous. The conclusion of immobile adsorbed CO_2 molecules is based on the assumption of an instantaneous adsorption rate and supports the opinion of Prasher and Ma (1977), who concluded that surface diffusion is an unlikely transport mechanism in liquid filled pores. However, a finite adsorption rate of CO_2 and a surface diffusion coefficient larger than zero could probably also result in the same agreement between theory and experiment. Nevertheless, the present model is able to describe the absorption behaviour of CO_2 in liquid impregnated γ-alumina particles sufficiently accurate.

Table 4. Diffusivity of gases in liquids at 298 K

Gas	Solvent	$D \times (10^{-9}\ m^2\ s^{-1})$	Source
CO_2	Ethanol	4.07	Snijder (1994)
CO_2	Toluene	4.89	Snijder (1994)
CO_2	Water	1.91	Versteeg (1988)
N_2O	Ethanol	4.25	Snijder (1994)
N_2O	Toluene	5.08	Snijder (1994)
N_2O	Water	1.78	Versteeg (1988)
N_2O	2 M MDEA	1.00	Versteeg (1988)

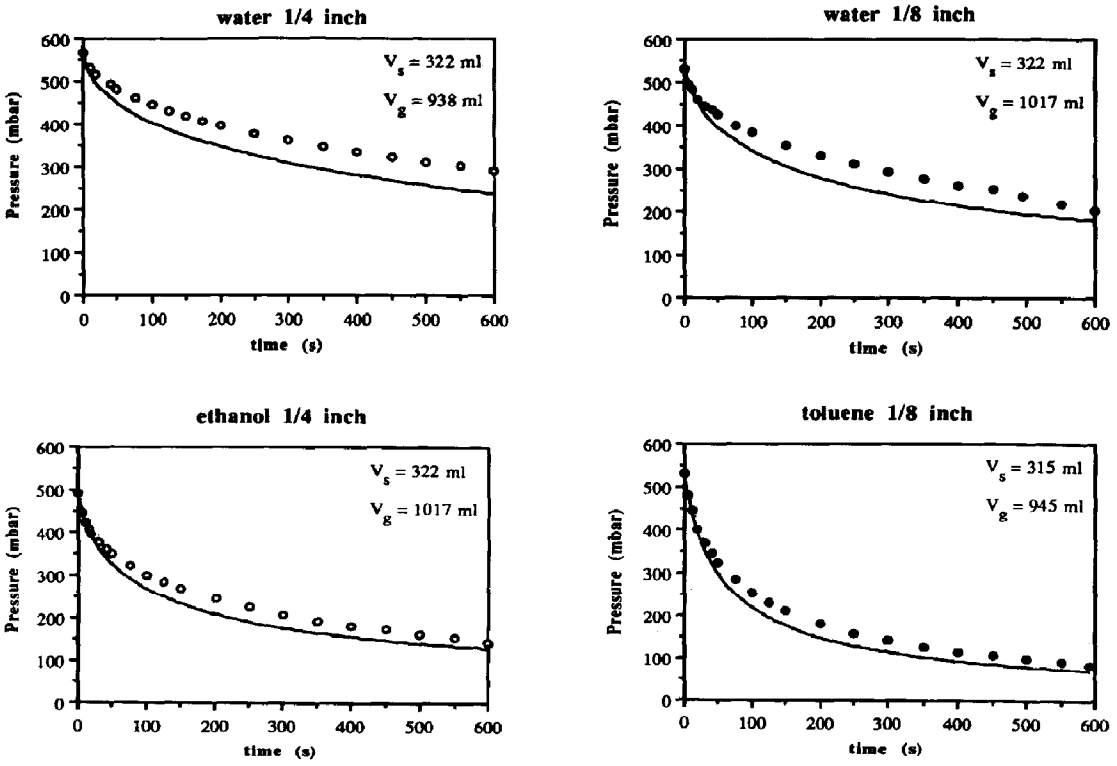

Fig. 9. CO_2 absorption rate at 298 K in γ-alumina particles impregnated with non-reacting liquids.

6. ABSORPTION RATE EXPERIMENTS IN REACTIVE SOLUTIONS

6.1. *Introduction*

First the absorption of CO_2 in various alkanolamine solutions will be treated (Section 6.2) whereafter the absorption of H_2S in the tertiary alkanolamine MDEA (Section 6.3) will be dealt with. In Section 6.4 some qualitative remarks will be made about the possibility and influence of surface adsorption of the reaction products on the absorption rate.

6.2. *Absorption rate of CO_2 in particles impregnated with alkanolamine solutions*

6.2.1. *Introduction.* Before discussing the experimental results of the absorption rates of CO_2 in particles impregnated with various alkanolamine solutions (Section 6.2.3), some theoretical absorption rates and concentration profiles in the particles will be given in Section 6.2.2.

6.2.2. *Influence of surface adsorption and parallel reactions.* In Section 6.2.2.1 the influence of immobile surface adsorption of CO_2 on the absorption rate of CO_2 in particles filled with the primary alkanolamine MEA is discussed, while in Section 6.2.2.2 the influence of reaction (21)–(24) on the absorption rate for CO_2 in particles impregnated with tertiary alkanolamines will be dealt with. Also, in Section 6.2.2.2 the influence of the surface adsorption of CO_2 in particles impregnated with tertiary alkanolamines is discussed. Finally, in Section 6.2.2.3 it will be demonstrated that the influence of surface adsorption and parallel reaction on the present absorption rate experiments is small.

6.2.2.1. Primary alkanolamines

Absorption rate experiments of CO_2 in γ-alumina particles indicated that the adsorbed CO_2 molecules were immobile. The effect of CO_2 adsorption on the absorption rate in particles impregnated with a MEA solution at a constant pressure is given in Table 5. The required input parameters were taken from literature and summarized in Tables 1 and 8. In Table 5 the dimensionless accumulation is the amount of gas which is absorbed at a particular time divided by the maximum amount which is absorbed at equilibrium. From this table it can be concluded that surface adsorption has for the CO_2–MEA system a decreasing influence with increase in time and diameter of the particles. For short times and small particles the flux is substantially higher as a consequence of the instantaneous nature of the adsorption reaction and the small diffusion distances which have to be travelled through the liquid. Although the fluxes for the situations with surface adsorption are always higher than without surface adsorption, the dimensionless accumulation at comparable times is, except for very small dimensionless accumulations, always lower. This is due to the fact that the CO_2 molecules which adsorb on the surface have to be transported through the liquid phase. This increases the CO_2 gradient and thereby the flux, but the saturation time is increased. It should be noted however, that the total absorption capacity is about 45% higher for the situation with surface adsorption.

6.2.2.2. Tertiary alkanolamine solutions

As mentioned earlier (Section 2.3) the influence of the reaction (21)–(24) on the CO_2 absorption rate for tertiary alkanolamines sometimes may be negligible.

Table 5. Influence of surface adsorption on the absorption rate of CO_2 for particles of 70 μm and 6 mm impregnated with a 2 M MEA solution at 298 K and a constant partial pressure of CO_2 of 10 mol m^{-3} (no gas phase resistance)

	70 μm				6 mm (multiply the time by 100)			
	Flux ($\times 10^{-3}$ mol m^{-2} s^{-1})		Accumulation (–)		Flux ($\times 10^{-3}$ mol m^{-2} s^{-1})		Accumulation (–)	
Time (s)	1	2	1	2	1	2	1	2
3.38×10^{-5}	15.6	48.0	1.46×10^{-4}	2.22×10^{-4}	12.3	15.1	8.94×10^{-5}	1.02×10^{-4}
1.56×10^{-5}	12.7	42.4	4.00×10^{-4}	8.02×10^{-4}	11.8	12.1	3.52×10^{-4}	2.96×10^{-4}
6.40×10^{-4}	12.5	28.6	1.32×10^{-3}	2.50×10^{-3}	10.9	11.0	1.30×10^{-3}	9.61×10^{-4}
2.16×10^{-3}	12.4	16.9	4.14×10^{-3}	5.76×10^{-3}	9.44	9.53	3.95×10^{-3}	2.8×10^{-3}
0.0100	11.9	12.5	0.0183	0.0168	6.47	6.54	0.0143	0.0100
0.0536	10.8	10.9	0.0913	0.0682	2.88	2.98	0.0452	0.0317
0.0926	10.1	10.2	0.1516	0.1104	2.12	2.20	0.0617	0.0435
0.2080	8.54	8.68	0.3105	0.2216	1.36	1.41	0.0948	0.0672
0.7147	3.98	4.35	0.7705	0.5501	0.69	0.72	0.175	0.125
1.406	0.63	1.67	0.9702	0.7440	0.46	0.49	0.242	0.173
2.500	0.02	0.66	0.9993	0.8612	0.33	0.35	0.312	0.227
4.477		0.24		0.9421	0.23	0.24	0.409	0.295
7.049		0.08		0.9802	0.16	0.18	0.496	0.358
10		0.02		0.9945	0.13	0.14	0.567	0.412

$q = 2.4$ $\varepsilon_p = 0.58$; for simulations with surface adsorption: $c_1 = 0.25$, $c_2 = 650$. 1 = without surface adsorption; 2 = surface adsorption included. The time for the 6 mm particles has to be multiplied by 100.

Maximum absorption capacity for the particles with surface adsorption (situation 2) is 45% larger than particles where no surface adsorption occurs (situation 1).

However, for small contact times, low CO_2 concentrations or high mass transfer coefficients some influence of reaction (21)–(24) can be observed (Glasscock and Rochelle, 1989). Therefore, for small particles, which are physically rapidly saturated, it may be possible that reaction (21)–(24) also influences the absorption rate. As can be seen for situations 1 and 2 in Table 6 [notice the plateau flux for situation 1, see Hogendoorn *et al.* (1993)] the influence of reaction (21)–(24) is especially observed for low CO_2 concentrations, whereas at higher CO_2 concentrations the effect of the extended reaction scheme is minor. The effect of surface adsorption is again most pronounced for short contact times. For a low CO_2 concentration the effect of reaction (21)–(24) can be observed even if surface adsorption occurs, while for high CO_2 concentrations this effect is much smaller (Table 6, situation 4). The dimensionless accumulation for the particles where surface adsorption occurs is comparable with the particles where no surface adsorption takes place for both reaction schemes. This is in contrast with the situation for MEA, and due to the low reaction rate constant of the CO_2–MDEA system: the rate of the CO_2 liquid transport necessary for the adsorption can, for small particles, keep pace with the reaction rate.

In case the diffusion lengths, i.e. particle diameter increase, the influence of surface adsorption decreases which can be seen in Table 7. For short times the flux for the situation with surface adsorption is still substantially higher than for the situation without surface adsorption, but with increasing time and thus diffusion lengths, the differences between the fluxes for situations 1 and 3 are, in comparison to the situation for small particles (Table 6), small. This can also be seen from the dimensionless accumulation, which was, for small particles for the situation with and without surface adsorption, comparable, while for the large particles the dimensionless accumulation for the situation with surface adsorption is always smaller. Also, for large particles the influence of reaction (21)–(24) diminishes strongly (situations 1 and 2, Table 7). The

Table 6. Influence of reaction (21)–(24) and surface adsorption on the absorption rate of CO_2 for particles of 70 μm impregnated with a 2 M MDEA solution at 298 K and a constant partial pressure of CO_2 (no gas phase resistance)

	Flux				Accumulation			
Time (s)	1	2	3	4	1	2	3	4
$[CO_2] = 0.01$ mol m^{-3}†								
3.375×10^{-4}	24.1	24.2	275	275	6.53×10^{-6}	6.55×10^{-6}	4.30×10^{-5}	4.30×10^{-5}
1.563×10^{-3}	11.4	11.7	175	175	1.34×10^{-5}	1.35×10^{-5}	1.36×10^{-4}	1.36×10^{-4}
6.400×10^{-3}	5.71	6.39	77.3	77.3	2.67×10^{-5}	2.77×10^{-5}	3.22×10^{-4}	3.22×10^{-4}
0.0216	3.38	4.51	40.3	40.4	5.00×10^{-5}	5.61×10^{-5}	6.06×10^{-4}	6.07×10^{-4}
0.100	2.31	4.00	18.4	18.7	1.24×10^{-4}	1.72×10^{-4}	1.31×10^{-3}	1.31×10^{-3}
0.536	2.19	3.98	7.91	8.40	4.74×10^{-4}	7.98×10^{-4}	3.00×10^{-3}	3.07×10^{-3}
0.926	2.19	3.97	6.05	6.69	7.84×10^{-4}	1.37×10^{-3}	3.95×10^{-3}	4.09×10^{-3}
2.080	2.19	3.95	4.18	5.08	1.70×10^{-3}	3.02×10^{-3}	5.95×10^{-3}	6.41×10^{-3}
7.147	2.19	3.86	2.70	3.99	5.75×10^{-3}	0.0102	0.0116	0.0141
14.06	2.19	3.75	2.36	3.69	0.0112	0.0197	0.0177	0.0234
25.00	2.19	3.59	2.23	3.44	0.0204	0.0342	0.0265	0.0372
44.77	2.19	3.36	2.20	3.15	0.0357	0.0592	0.0419	0.0601
70.49	2.18	3.13	2.19	2.92	0.05625	0.0892	0.0617	0.0875
100.0	2.18	2.95	2.18	2.77	0.07978	0.1215	0.0842	0.1181
$[CO_2] = 10$ mol m^{-3}‡								
3.375×10^{-4}	24.1	24.2	229	229	2.79×10^{-4}	2.80×10^{-4}	1.17×10^{-3}	1.17×10^{-3}
1.563×10^{-3}	11.4	11.7	113	113	5.71×10^{-4}	5.78×10^{-4}	3.17×10^{-3}	3.17×10^{-3}
6.400×10^{-3}	5.71	6.25	49.9	50.0	1.14×10^{-3}	1.19×10^{-3}	6.74×10^{-3}	6.78×10^{-3}
0.0216	3.38	4.02	26.7	26.9	2.12×10^{-3}	2.32×10^{-3}	0.0124	0.0125
0.100	2.31	2.77	12.3	12.4	5.28×10^{-3}	6.17×10^{-3}	0.0266	0.0269
0.536	2.18	2.33	5.35	5.48	0.0202	0.0228	0.0613	0.0624
0.926	2.17	2.26	4.18	4.28	0.0333	0.0368	0.0809	0.0826
2.080	2.14	2.18	3.05	3.12	0.0718	0.0767	0.1234	0.1271
7.147	1.97	1.97	2.24	2.25	0.2337	0.2404	0.2609	0.2662
14.06	1.67	1.66	1.93	1.92	0.4296	0.4362	0.4153	0.4209
25.00	1.14	1.12	1.48	1.46	0.6677	0.6726	0.6159	0.6206
44.77	0.42	0.41	0.72	0.71	0.8928	0.8956	0.8447	0.8478
70.49	0.08	0.08	0.20	0.20	0.9809	0.9796	0.9608	0.9615
100.0	0.01	0.01	0.04	0.04	0.9971	0.9971	0.9926	0.9928

† Flux in units of 10^{-7} mol m^{-2} s^{-1}.
If surface adsorption occurs (situations 3 and 4) the maximum capacity is increased by 3% in comparison with situations 1 and 2.

‡ Flux in units of 10^{-4} mol m^{-2} s^{-1}.
If surface adsorption occurs (situations 3 and 4) the maximum capacity is increased by 4% in comparison with situations 1 and 2.

$q = 2.4$ $\varepsilon_p = 0.58$; for simulations with surface adsorption: $c_1 = 0.25$, $c_2 = 650$. 1 = only reaction (20); 2 = reactions (20)–(24); 3 = only reaction (20) with surface adsorption; 4 = reactions (20)–(24) and surface adsorption.

Table 7. Influence of reaction (21)–(24) and surface adsorption on the absorption rate of CO_2 for particles of 6 mm impregnated with a 2 M MDEA solution at 298 K and a constant partial pressure of CO_2 of 10 mol m^{-3} (no gas phase resistance)

	Flux ($\times 10^{-4}$ mol m^{-2} s^{-1})				Accumulation			
Time (s)	1	2	3	4	1	2	3	4
$[CO_2] = 0.01$ mol m^{-3}†								
3.375×10^{-3}	7.98	8.43	72.0	72.1	1.06×10^{-6}	1.09×10^{-6}	6.20×10^{-6}	6.22×10^{-6}
0.01563	4.26	4.89	32.0	32.1	2.27×10^{-6}	2.45×10^{-6}	1.29×10^{-5}	1.30×10^{-5}
0.0640	2.91	3.48	16.0	16.1	5.21×10^{-6}	5.94×10^{-6}	2.56×10^{-5}	2.59×10^{-5}
0.216	2.64	2.99	8.88	9.06	1.28×10^{-5}	1.47×10^{-5}	4.72×10^{-5}	4.78×10^{-5}
1.00	2.62	2.75	4.58	4.71	5.02×10^{-5}	5.51×10^{-5}	1.05×10^{-4}	1.07×10^{-4}
5.36	2.58	2.62	2.91	2.97	2.56×10^{-4}	2.67×10^{-4}	2.87×10^{-4}	2.95×10^{-4}
9.26	2.55	2.58	2.72	2.76	4.38×10^{-4}	4.52×10^{-4}	4.23×10^{-4}	4.34×10^{-4}
20.80	2.50	2.51	2.57	2.59	9.66×10^{-4}	9.87×10^{-4}	8.01×10^{-4}	8.18×10^{-4}
71.47	2.31	2.31	2.38	2.38	3.17×10^{-3}	3.20×10^{-3}	2.36×10^{-3}	2.38×10^{-3}
140.6	2.11	2.10	2.20	2.20	5.93×10^{-3}	5.97×10^{-3}	4.33×10^{-3}	4.36×10^{-3}
250.0	1.87	1.86	1.99	1.99	9.87×10^{-3}	9.91×10^{-3}	7.18×10^{-3}	7.21×10^{-3}
447.7	1.56	1.55	1.72	1.72	0.0159	0.0160	0.0117	0.0118
704.9	1.29	1.28	1.48	1.47	0.0226	0.0226	0.0168	0.0171
1000	1.07	1.07	1.27	1.27	0.0288	0.0289	0.0219	0.0219

†If surface adsorption occurs (situations 3 and 4) the maximum capacity is increased with 44% in comparison with situations 1 and 2.

$q = 2.4$ $\varepsilon_p = 0.58$; for simulations with surface adsorption: $c_1 = 0.25$, $c_2 = 650$. 1 = only reaction (20); 2 = reactions (20)–(24); 3 = only reaction (20) with surface adsorption; 4 = reactions (20)–(24) with surface adsorption.

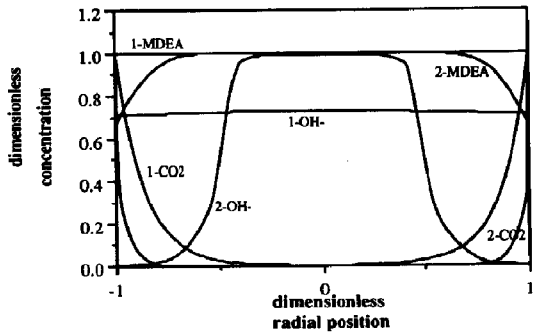

Fig. 10. Concentration profiles of CO_2, OH^- and MDEA inside the particle at a dimensionless accumulation of 0.0197 (–). For both situations the absorption in 2 M MDEA solution is considered with $\varepsilon_p = 0.58$, $1 = 2.4$. Situation (1) $[CO_{2,gas}] = 0.01$ mol m^{-3}, $r_1 = 35$ μm, $t = 14.06$ s. Situation (2) $[CO_{2,gas}] = 10$ mol m^{-3}, $r_1 = 3$ mm, $t = 582$ s. Scaling: $OH^- = 1 \approx 2.3$ mol m^{-3}; MDEA $= 1 \approx 2000$ mol m^{-3}; situation (1) $CO_2 = 1 \approx 7.2 \times 10^{-3}$ mol m^{-3}; situation (2) $CO_2 = 1 \approx 7.2$ mol m^{-3}.

CO_2, OH^- and MDEA concentration profiles for the small and large particles at about the same dimensionless accumulation are given in Fig. 10. As expected, the concentration OH^- decreases rapidly near the interface for large particles, thereby reducing the influence of reaction (21) on the absorption rate. In contrast, the concentration OH^- in small particles remains practically constant over the entire radius of the particles, thereby influencing the absorption behaviour significantly.

These simulations show that for small particles with short residence times, e.g. risers or trickle flow reactors, special attention must be paid to reaction (21)–(24) and the surface adsorption.

6.2.2.3. Influence of parallel reactions and surface adsorption on the time–pressure curves

The present absorption rate experiments were carried out with large alumina particles, initially high CO_2 concentrations and large contact times in the reactor. Under these circumstances the influence of both reaction (21)–(24) for tertiary alkanolamines and surface adsorption in γ-alumina particles is relatively small as was demonstrated in Sections 6.2.2.1 and 6.2.2.2. To verify whether either reaction (21)–(24) or the surface adsorption reaction had any noticeable effect on the time–pressure curves some comparative simulations were carried out for typical experimental conditions.

The absorption of CO_2 in porous α-alumina particles impregnated with a 2 M aqueous MDEA solution at 298 is given in Fig. 11. Both the simplified [only reaction (20)] and the extended reaction scheme [reaction (20)–(24)] were used in these calculations. From the results presented in Fig. 11 it can be seen that neglecting reaction (21)–(24) have very little influence on the time–pressure curve. Therefore, it was concluded that the actual experiments with tertiary alkanolamines could be interpreted on the basis of reaction (20). The equilibrium value of this reaction, K_{CO_2}, was comprised of the equilibrium values of reactions (21), (23) and (24) and defined as

$$K_{CO_2} = \frac{K_1 K_w}{K_a}[H_2O]. \qquad (32)$$

The influence of surface adsorption of CO_2 on the time–pressure curve for typical experimental conditions with γ-alumina particles is for both 2 M MEA as well as 2 M MDEA given in Fig. 12. In this figure it can be observed that the influence of surface adsorp-

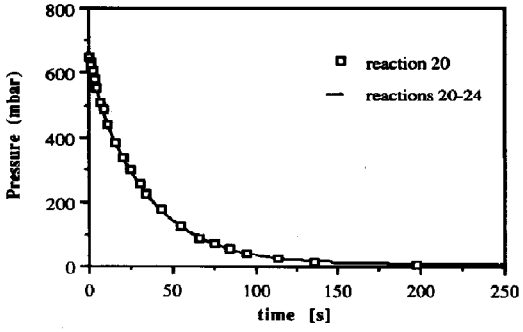

Fig. 11. Comparison for the absorption of CO_2 in a 2 M MDEA solution at 298 K for the extended and simplified reaction scheme.

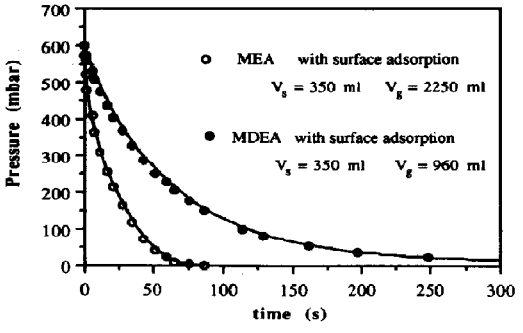

Fig. 12. Influence of surface adsorption on the CO_2 absorption rate at 298 K for $\frac{1}{8}$ in γ-alumina particles impregnated with 2 M aqueous alkanolamine solutions.

tion on the time–pressure curve is, even for the slowly reacting MDEA solution, very small. As already demonstrated this is due to the large particles, long contact but also to the fact that the gas concentration decreases. If the gas concentration decreases, the instantaneously adsorbed gas molecules just inside the particle will desorb and penetrate further inside the particle. This means that the effect of the instantaneous surface adsorption at decreasing gas concentration is smaller as compared to the situation with a constant gas concentration.

In the simulations of the absorption rate experiments, surface adsorption was for the γ-alumina particle always taken into account. For tertiary alkanolamines and all particles the experiments were simulated neglecting reaction (21)–(24). One should remember that the marginal effect of both reaction (21)–(24) and the surface adsorption on the time–pressure curves is only due to the experimental conditions (large particles, high CO_2 concentrations, long contact times, decreasing pressure), and that for other experimental conditions these two may well influence the absorption rate.

6.2.3. *Experimental absorption rate experiments of CO_2 in alkanolamine solutions.* Typical results for the

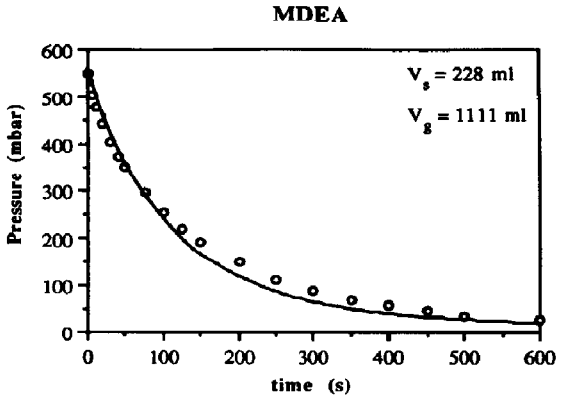

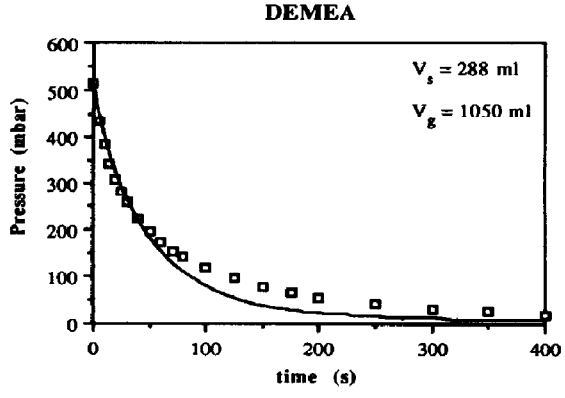

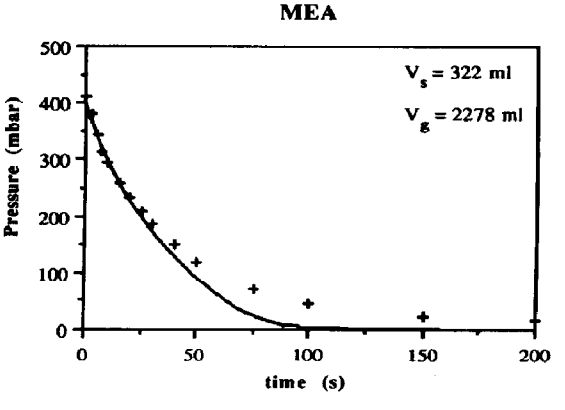

Fig. 13. CO_2 absorption rate at 298 K in α-alumina particles impregnated with aqueous 2 M aqueous alkanolamine solutions.

absorption rate experiments of CO_2 in α-alumina pellets impregnated with alkanolamine solutions are given in Fig. 13. The continuous line represents the numerically calculated partial pressures, while the points are the experimentally determined partial pressures. It should be emphasized that the parameters required for the calculations were taken from liter-

Table 8. Physical constants in 2 M aqueous alkanolamine solutions at 298 K

Physical constant	MDEA	DEMEA	MEA
m_{N_2O}	0.51 (Littel, 1991b)	0.54 (Littel, 1991b)	0.63 (Versteeg, 1988)
Viscosity (Pa s)	2.20×10^{-3} (Littel, 1991b)	2.71×10^{-3} (Littel, 1991b)	1.3×10^{-3} (Versteeg, 1988)
D_{amine} ($m^2 s^{-1}$)	4.56×10^{-10} (Snijder, 1993)	†	9.07×10^{-10} (Versteeg, 1988)
$k_{1,1}$ ($m^3 mol^{-1} s^{-1}$)	5.2×10^{-3} (Littel, 1990b)	4.34×10^{-2} (Littel, 1990b)	5.70 (Blauwhoff, 1984)

†Calculated with Wilke Chang and modified Stokes–Einstein relationship (Versteeg, 1988). Solubility of CO_2 calculated with "N_2O–CO_2" analogy (Laddha, 1981). Diffusivity of CO_2 in aqueous alkanolamine solution calculated with modified Stokes–Einstein relationship (Versteeg, 1988).

ature (see Tables 1 and 8) and that no fit procedure was applied to simulate the experiments.

For the comparison of the experiments with the simulations for the γ-alumina particles, the adsorption of CO_2 in γ-alumina particles impregnated with aqueous alkanolamine solutions was taken into account. It was assumed that the Langmuir adsorption isotherm was not affected by the presence of the alkanolamines and could be described by the constants given in Fig. 2. This assumption is based on the experimental observation that the summation of the Langmuir adsorption isotherm and the absorption data of CO_2 in a homogeneous aqueous MDEA solution agree reasonably with the absorption data of CO_2 in γ-alumina particles impregnated with a MDEA solution (see Fig. 6). In Fig. 14 typical examples of the absorption rate of CO_2 in γ-alumina particles of $\frac{1}{4}$ in impregnated with alkanolamine solutions are presented. In Fig. 15 results are given for the particles of $\frac{1}{8}$ in. The agreement between theory and experiment for all alkanolamines is satisfactory in the range from the initial pressure to about 100 mbar. However, below 100 mbar the solvent becomes substantially converted and equilibrium is approached. The liquid composition increasingly influences the absorption rate in this area. For all amines, but especially for MEA, substantial deviations between theoretical and experimental absorption behaviour were obtained in this area. Three possible causes for these deviations can be presented:

— The neglection of the influence of non-idealities on the equilibrium composition. Although the total liquid loading remains low, the assumption of ideal behaviour of all components may be incorrect.

— The value of the equilibrium constant used in the simulations could be inaccurate. If the overall equilibrium constant for the CO_2–MEA reaction [eq. (25)] in the simulation was lowered from 39.4 (according to Table 1) to 5, the agreement between experiment and simulation in the range from 0 to 100 mbar was already much better. This decrease of the equilibrium constant for MEA leads to a reduction of about 50% of the absorption capacity at very low (< 0.05 mol m^{-3}) partial pressures, while the decrease in absorption capacity at higher (> 2 mol m^{-3}) partial pressures is less than 10%. Such a variation of the equilibrium constant is realistic, because owing to impurities in the alkanolamines or differences in the experimental set-up, the equilibrium data reported in literature scatter substantially for especially low gas concentrations (see, e.g. Fig. 5 for MDEA). Bosch *et al.* (1989a) studied the desorption of CO_2 from loaded MEA solutions, and although non-idealities were incorporated in the equilibrium model, the predicted CO_2 fluxes from the MEA solutions differed substantially from the experimental fluxes. Bosch *et al.* (1989a) also supposed that the equilibrium model was not sufficiently accurate to simulate the desorption.

— The deviations for the tertiary amines (MDEA and DEMEA) in the range from 0 to 100 mbar are in general less severe as for the primary amine MEA. The reason for this larger deviation for MEA can be due to the difference in the reaction scheme between the two types of amines. In the calculation of the equilibrium composition for the system CO_2 and aqueous MEA the hydrolysis of the carbamate ($MEACOO^-$) according to reaction (27) was taken into account. However, the rate of this reaction is relatively low (Danckwerts and McNeil, 1967) and will probably only be of importance for longer contact times. Consequently, the hydrolysis of the carbamate should be neglected for the absorption rate experiments with MEA. Therefore, it may be concluded that in the simulations the MEA concentration is overestimated, resulting in a too high absorption rate.

6.2.4. *Absorption rate experiments of* H_2S *in a MDEA solution.* The results for the absorption rate experiments of H_2S in particles impregnated with MDEA solutions are given in Fig. 16. Because the reaction of H_2S with MDEA is infinitely fast in comparison with the mass transport, the reaction can be considered at equilibrium at any place within the particle. This means that the equilibrium value has a great impact on the absorption rate. Therefore, it was preferred to use the own experimentally found equilibrium value ($K_{H_2S} = 18$, see Fig. 8) in the simulations instead of the data from literature (see Section 4.1.2). In the simulations of the experiments with γ-alumina the immobile surface adsorption was also taken into account. It was assumed that the surface

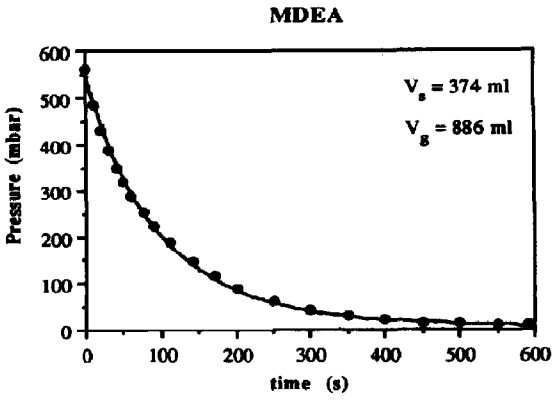

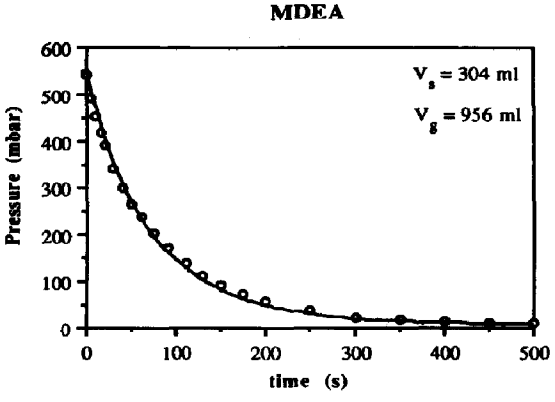

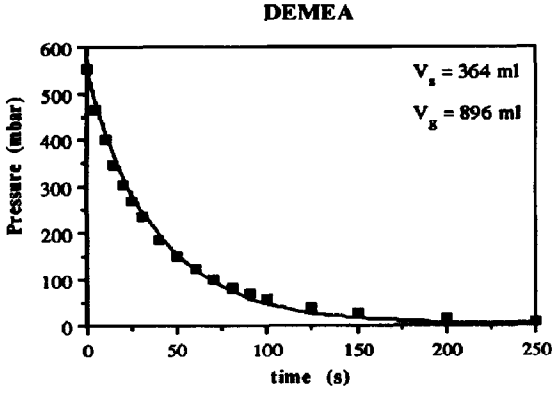

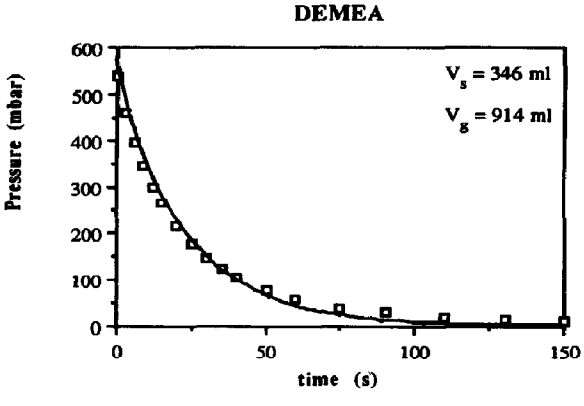

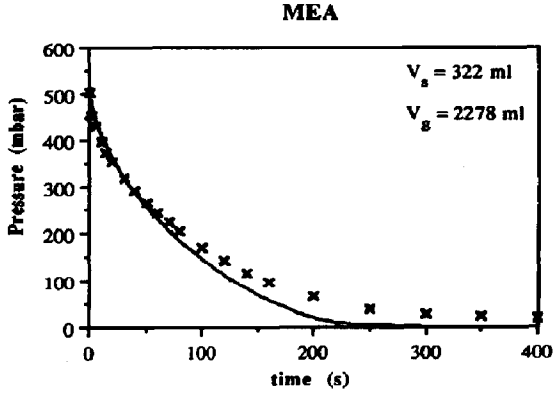

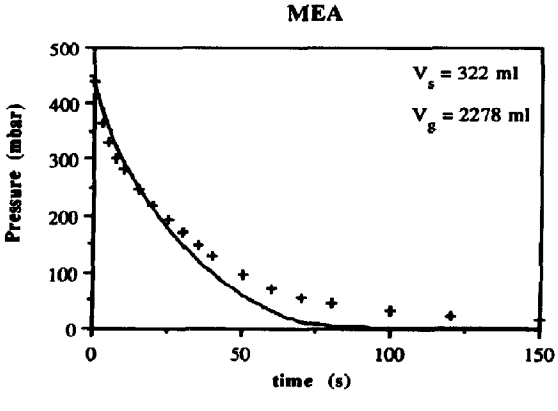

Fig. 14. CO_2 absorption rate at 298 K in $\frac{1}{4}$ in γ-alumina particles impregnated with aqueous 2 M alkanolamine solutions.

Fig. 15. CO_2 absorption rate at 298 K in $\frac{1}{8}$ in γ-alumina particles impregnated with aqueous 2 M alkanolamine solutions.

adsorption isotherm of H_2S in γ-alumina particles impregnated with MDEA solutions could be described by the isotherm found for water impregnated γ-alumina particles (see Fig. 4). Contrary to the absorption rate experiments for the CO_2 in γ-alumina pellets, the simulations indicate that surface adsorption has a slight influence on the time–pressure curves. The cause for this influence of surface adsorption is due to the relatively low equilibrium constant for the H_2S–MDEA system. The tortuosity used in the simulations was adopted from the physical absorption rate experiments as described in Sections 5.2 and 5.3. This means that these experiments were also simulated without the introduction of any additional fit parameters. The data required for the simulation are given in Table 9. The experimental absorption rates of H_2S

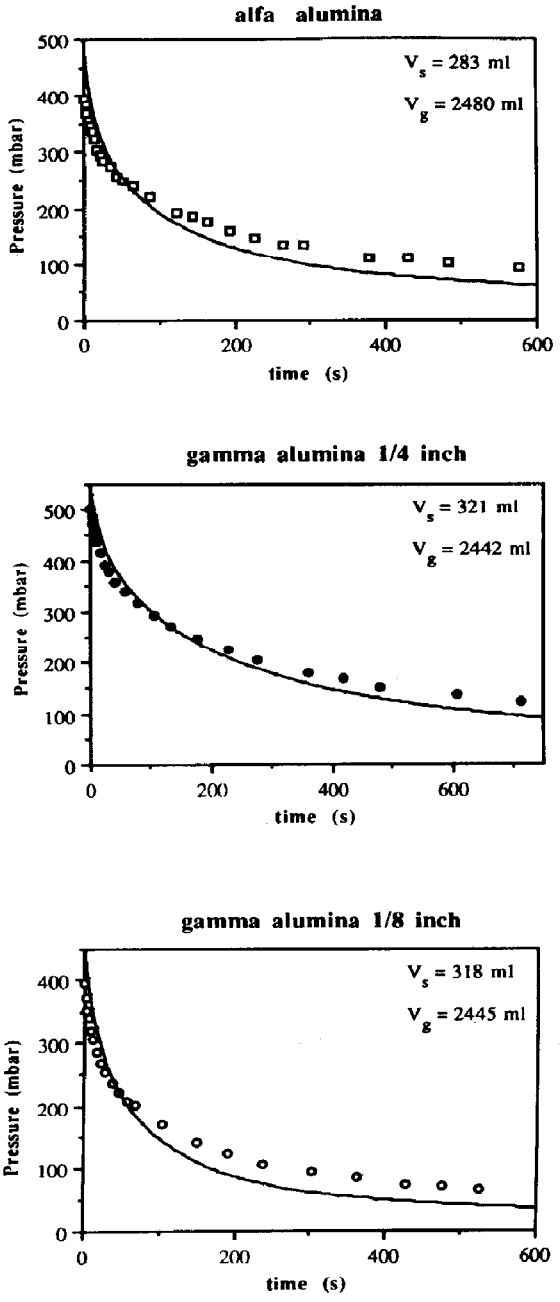

Fig. 16. H_2S absorption rate at 298 K in 2 M MDEA solutions in various alumina carriers.

in various particles show the same type of deviation. For short times the theory predicts absorption rates which are too low, while for longer times the absorption rates for all pellets is somewhat faster as measured experimentally. This systematic deviation is probably still due to equilibrium value (see Fig. 8) which is not able to predict the equilibrium data accurately over the whole H_2S concentration range.

Table 9. Parameters for the H_2S and 2 M MDEA system at 298 K

Parameters	References
$m_{H_2S} = 2.17$	Versteeg *et al.*, 1989
$K_{H_2S} = 18$	This work
$D_{H_2S} = 9.27 \times 10^{-10}$	Versteeg *et al.*, 1989
$D_{MDEA} = 4.37 \times 10^{-10}$	Versteeg *et al.*, 1988

Diffusivity and solubility of H_2S were estimated analogous to the "CO_2–N_2O" analogy (Versteeg *et al.*, 1989).

Nevertheless, the agreement between theory and experiments is reasonable.

6.3. *Influence of surface adsorption of the reaction products on the absorption rate*

Analysis of the composition of the aqueous MDEA solution before and after the impregnation of the γ-alumina particles resulted in identical concentrations of MDEA. This means that adsorption of MDEA on the internal surface of γ-alumina is very small. No experimental data are known for the adsorption of the products of the reaction between CO_2 or H_2S and the various alkanolamines on the internal surface. Because the absorption data of CO_2 in γ-alumina impregnated with MDEA correspond reasonably well with the sum of the absorption data of CO_2 in γ-alumina impregnated with water and the absorption data of Jou *et al.* (1982), it can be assumed that the products do not strongly adsorb on the surface. However, it cannot be excluded that the surface adsorption of CO_2 decreases in the presence of the products of the CO_2-alkanolamine reaction.

The influence of surface adsorption of the products on the absorption rate of the gas will increase with the ratio of the amount adsorbed products on the surface to the equilibrium constant. Due to possible surface adsorption of the products the equilibrium constant can apparently be increased. For reactions of finite rate the equilibrium value only influences the absorption rate of the gas at longer times (see Hogendoorn *et al.*, 1993). However, for reactions instantaneous with respect to mass transfer, possible adsorption of the reaction products will influence the absorption behaviour from the start of the experiment. Because the surface adsorption of the reaction products is expected to be low, it will probably have, just like the surface adsorption of CO_2 and H_2S, a limited effect on the time–pressure curve for the absorption of CO_2 in alkanolamine solutions.

7. CONCLUSIONS

An experimental study of the absorption behaviour of CO_2 and H_2S in α-alumina and γ-alumina particles impregnated with non-reactive and reactive solvents is presented. Physical absorption rate experiments of CO_2 and N_2O were carried out to obtain the tortuosity of the porous materials. The tortuosity of the pores of the α-alumina particles and γ-alumina particles

were, respectively, 2.0 ± 0.3 and 2.4 ± 0.3. All additional parameters required for the simulation of the absorption of CO_2 and H_2S in alkanolamine solutions were taken from literature. The absorption of CO_2 and H_2S in α-alumina particles impregnated with these solutions could be described satisfactorily. Differences between experiments and simulations for CO_2 mainly occurred at approaching equilibrium and seemed to be primarily caused by the inaccuracy of the equilibrium composition of the CO_2-alkanolamine system. An unexpected immobile surface adsorption of CO_2 and H_2S was observed in γ-alumina particles impregnated with reactive as well as non-reactive solvents. However, this surface adsorption did not influence the absorption rate of CO_2 and H_2S in γ-alumina particles impregnated with alkanolamine solutions significantly. The rate of CO_2 and H_2S absorption in γ-alumina particles impregnated with alkanolamine solutions could, like the experiments with α-alumina, also be described within a reasonable accuracy.

NOTATION

a_s specific contact area between gas and solid, $m^2\,m^{-3}$
[A] concentration of absorbed component, $mol\,m^{-3}$ liquid
$[A]_{ads}$ concentration of adsorbed component, $mol\,m^{-3}$ liquid
[B], [C], [D] concentration of non-volatile reactants and products, $mol\,m^{-3}$ liquid
c_1 constant in eq. (4), $m^3\,mol^{-1}$
c_2 constant in eq. (4), $mol\,m^{-3}$ liquid
D diffusion coefficient, $m^2\,s^{-1}$
d diameter particle, m
J_a flux of absorbed component A, $mol\,m^{-2}\,s^{-1}$
K equilibrium constant, $(mol\,m^{-3})^{-n-m+p+q}$
$k_{n,m}$ forward reaction rate constant, $(mol\,m^{-3})^{(-n-m+1)}\,s^{-1}$
$k_{p,q}$ reverse reaction rate constant, $(mol\,m^{-3})^{(-p-q+1)}\,s^{-1}$
l length cylindrical particles m
m_a partition coefficient of A
P pressure, bar
q tortuosity
r_1 radius of particle, m
r radial coordinate, m
R_A reaction rate related to component A, $mol\,m^{-3}$ liquid s^{-1}
R gas constant, $J\,mol^{-1}\,K^{-1}$
T temperature, K
t time, s
V_{gas} volume occupied by gas in absorption vessel, m^3
V_{tot} total volume of absorption vessel, m^3
V_s volume occupied by liquid impregnated particles, m^3

Greek letters

ε_s fraction of total volume occupied by liquid impregnated particles
ε_p porosity
γ_i stoichiometric coefficient in relation (1)

Superscripts

n, m, p, q reaction orders in reaction rate expression R_1
0 initial

REFERENCES

Aris, R., 1957, On shape factors for irregular particles I—The steady state problem. Diffusion and reaction. *Chem. Engng Sci.* **6**, 262–268.

Bhairi, A. M., 1984, Experimental equilibrium between acid gases and ethanolamine solutions. Ph.D. dissertation, Oklahoma State University.

Blauwhoff, P. M. M. and Swaaij van, W. P. M., 1980, Gas–liquid equilibria between H_2S, CO_2 and aqueous amine solutions, in *Proceedings of 2nd International Conference on Phase Equilibria and Fluid properties in the Chem. Ind.*, p. 78. EFCE publication 11, Berlin.

Blauwhoff, P. M. M., Versteeg, G. F. and Swaaij van, W. P. M., 1984, A study on the reaction between CO_2 and alkanolamines in aqueous solutions. *Chem. Engng Sci.* **39**, 207–225.

Bosch, H., Versteeg, G. F. and Swaaij van, W. P. M., 1989a, Desorption of acid gases from loaded alkanolamine solutions, in *Proceedings of Process Technology, Vol. 8, Gas Separation and Purification*, pp. 505–512. Antwerpen.

Bosch, H., Versteeg, G. F. and Swaaij van, W. P. M., 1989b, A centrifugal reactor for the selective removal of H_2S from CO_2 containing gases, in *Proceedings of Process Technology, Vol. 8, Gas Separation and Purification*, pp. 513–520. Antwerpen.

Crank, J., 1976, *Mathematics of diffusion*, reprint. Oxford University Press, Oxford.

Danckwerts, P. V. and McNeil, K. M., 1967, The absorption of carbon dioxide into aqueous amine solutions and the effect of catalysis. *Trans. Instn. Chem. Engrs.* **45**, T32–T49.

Edeskuty, F. J. and Amundson, N. R., 1952, Effect of intra particle diffusion—agitated non flow adsorption systems. *Ind. Engng Chem.* **44**, 1698–1703.

Glasscock, D. A. and Rochelle, G. T., 1989, Numerical simulation of theories of gas absorption with chemical reaction. *A.I.Ch.E. J.* **35**, 1271–1281.

Hogendoorn, J. A., Versteeg, G. F. and Swaaij van, W. P. M., 1993, Mass transfer accompanied by reversible chemical reactions in an inert porous sphere impregnated with a stagnant liquid. *Chem. Engng Sci.* **48**, 2727–2740.

IUPAC, 1981, *Solubility Data Series, Vol. 8, Oxides of Nitrogen* (Edited by L. Young). Pergamon Press, Oxford.

Jou, F. Y., Mather, A. E. and Otto, F. D., 1982, Solubilities of H_2S and CO_2 in aqueous methyldiethanolamine solutions. *Ind. Engng Chem. Process Des. Dev.* **21**, 539–544.

Komiyama, H. and Smith, J. M., 1974a, Intraparticle mass transfer in liquid-filled pores. *A.I.Ch.E. J.* **20**, 728–734.

Komiyama, H. and Smith, J. M., 1974b, Surface diffusion in liquid filled pores. *A.I.Ch.E. J.* **20**, 1110–1117.

Laddha, S. S., Diaz, J. M. and Danckwerts, P. V., 1981, The N_2O analogy: the solubilities of CO_2 and N_2O in aqueous solutions of organic compounds. *Chem. Engng Sci.* **36**, 228–229.

Lee, S. Y., Seader, J. D., Tsai, C. H. and Massoth, F. E., 1993, Multicomponent liquid-phase diffusion and adsorption in porous catalyst particles. *Chem. Engng Sci.* **48**, 595–607.

Leyva-Ramos, R. and Geankoplis, C. J., 1985, Model simulation and analysis of surface-diffusion of liquids in porous solids. *Chem. Engng Sci.* **50**, 799–807.

Littel, R. J., Boss, M. and Knoop, G. J., 1990a, Dissociation constants of some alkanolamines at 293, 303, 318 and 333 K. *J. chem. Engng Data* **35**, 276–277.

Littel, R. J., Filmer, B., Versteeg, G. F. and Swaaij van, W. P. M., 1991a, Modelling of the simultaneous absorp-

tion of H_2S and CO_2 in alkanolamine solutions: the influence of parallel and consecutive reversible reactions and the coupled diffusion of ionic species. *Chem. Engng Sci.* **46**, 2303–2313.

Littel, R. J., Swaaij van, W. P. M. and Versteeg, G. F., 1990b, The kinetics of carbon dioxide with tertiary amines in aqueous solution. *A.I.Ch.E. J.* **36**, 1633–1640.

Littel, R. J., Versteeg, G. F. and Swaaij van, W. P. M., 1991b, Solubility and diffusivity data for the absorption of COS, CO_2 and N_2O in amine solutions. *J. chem. Engng Data* **37**, 49–55.

Littel, R. J., Versteeg, G. F. and Swaaij van, W. P. M., 1991c, Diffusivity measurements in some organic liquids by a gas–liquid diaphragm cell. *J. chem. Engng Data* **37**, 42–45.

Littel, R. J., Versteeg, G. F. and Swaaij van, W. P. M., 1991d, Physical absorption into non-aqueous solutions in a stirred cell reactor. *Chem. Engng Sci.* **46**, 3308–3313.

Ma, Y. H. and Evans, L. B., 1968, Transient diffusion from a well stirred reservoir to a body of arbitrary shape. *A.I.Ch.E. J.* **14**, 956–961.

Prasher, R. P. and Ma, Y. H., 1977, Liquid diffusion in microporous alumina pellets. *A.I.Ch.E. J.* **23**, 303–311.

Rosynek, M. P., 1975, Isotherms and energetics of carbon dioxide adsorption on γ-alumina at 100–300°C. *J. Phys. Chem.* **79**, 1280–1284.

Schrauwen, F. J. M. and Thoenes, D., 1988, Selective gas absorption in a spray cyclone scrubber. *Chem. Engng Sci.* **43**, 2189–2194.

Snijder, E. D., te Riele, M. J., Versteeg, G. F. and Swaaij van, W. P. M., 1993, Diffusion coefficients of several aqueous alkanolamine solutions. *J. Chem. Eng. Data*, **38**, 475–480.

Snijder, E. D., te Riele, M. J., Versteeg, G. F. and Swaaij van, W. P. M., 1994, Diffusion coefficients of CO, CO_2, N_2O and N_2 in ethanol and toluene. *J. Chem. Eng. Data* (submitted).

Versteeg, G. F. and Swaaij van, W. P. M., 1987, The gas–liquid centrifugal reactor. A novel type of gas–liquid contactor. *I. Chem. E. Symp. Series* **104**, B139–B154.

Versteeg, G. F. and Swaaij van, W. P. M., 1988, Solubility and diffusivity of acid gases (CO_2, N_2O) in aqueous alkanolamine solutions. *J. Chem. Engng Data* **33**, 29–34.

Versteeg, G. F., Kuipers, J. A. M., Beckum van, F. P. H. and Swaaij van W. P. M., 1989, Mass transfer with complex reversible reactions—I. Single reversible chemical reaction. *Chem. Engng Sci.* **44**, 2295–2310.